Incoherent Synthesis of Sparse Arrays for Frequency-Invariant Beamforming

Yaakov Buchris, *Member, IEEE*, Alon Amar, *Member, IEEE*, Jacob Benesty, and Israel Cohen, *Fellow, IEEE*

***Abstract*—Frequency-invariant beamformers are used to prevent signal waveform distortions in real world applications like audio, underwater acoustics, and radar. Most of existing methods assume uniform arrays, and only few consider sparse designs, which may lead to higher performance in terms of robustness and directivity factor. We propose an incoherent approach that first determines for each frequency bin a sparse set of sensors positions. Subsequently, by using tools of dimensionality reduction and clustering, these selections are merged together yielding the optimal sensors on a sparse array layout. We present design examples of sparse linear and planar superdirective array designs. We show that the proposed incoherent sparse design obtains superior performance in terms of white noise gain, directivity factor, and computational load compared to a uniform array design and compared to a coherent sparse approach, where the sensors' locations and the beamformer coefficients are optimized simultaneously for all frequencies.**

***Index Terms*—Frequency-invariant beamformer, sparse design, superdirective beamformers, differential microphone arrays.**

I. Introduction

DESIGN of nearly frequency-invariant (FI) broadband beamformers for several real-world applications like audio, communication, and sonar systems [1]–[3], is important as such beamformers can recover the signals of interest while reducing some artifacts caused by beamforming. Classical approaches of FI beamforming are based on constrained optimization [4]–[10], analytical solutions [11], [12], and coherent subspace methods [13]–[15]. Another concept is based on differential microphone arrays (DMAs) [16]–[23] and superdirective beamformers [24]. In all these former works, it was assumed that the sensors are located either uniformly or nonuniformly in a given aperture which can be linear, planar, or arbitrary. Yet, optimizing the number of sensors and/or their locations was not considered, and only the beamformer coefficients were optimized according to certain design constraints.

The shortcomings of the previous design opens a window of opportunities for a class of sparse methods which optimize also the number of sensors and their positions. In sparse arrays, also termed as aperiodic, random, thinned or space tapered arrays, the nonuniform design of the sensors' locations enables to obtain arrays where part of their adjacent sensors have spacing larger than half the wavelength. Yet, the harmful effects of grating lobes can be completely mitigated. Thus, arrays with a greater aperture and better robustness to array imperfections, but with a smaller number of sensors than in the uniform design, can be designed using the sparse approach. In the context of FI beamformers, sparsity may lead to more flexibility and better design in terms of satisfying constraints on a wider range of frequencies. Practically, sparse arrays can be integrated into several real-world applications where strong limitations are imposed on the weight, size, and cost of sensors.

While for the narrowband design many advanced techniques have been presented for the synthesis of sparse arrays [25]–[36], less work has been done for the sparse design of FI broadband beamformers. One simple sparse structure of FI beamforming is based on the concept of harmonic nested arrays [37], [38] where the total array is composed from several uniform subarrays, each matched to a different frequency subband. Yet, the locations of the sensors are set only according to the spatial sampling constraint in the relevant subband, and are not optimized according to some design constraints like robustness to mismatch errors.

Analytical approaches for optimization of the sensors positions in order to obtain FI beampattern can be found in [39], [40]. However, in these approaches no consideration regarding issues like robustness to noise has been done. This restricts to some extent the feasibility of such approaches in cases of small size arrays. Crocco and Trucco [41] proposed a FI sparse design by joint-optimization of the sensors positions and the beamformer coefficients, using simulated annealing optimization, while assuming a given a-priori number of sensors on the sparse array. In [42], a genetic algorithm combined with a gradient-based method was applied to find a global minimum for the optimization of the cost function. A design of FI beampattern for linear arrays based on the generalized matrix pencil method can be found in [43].

Recently, both Hawes and Liu [44], and Liu *et al*. [45] proposed sparse designs for broadband beamformers based on an iterative weighted ℓ_1-norm minimization under multiple convex

Manuscript received March 4, 2018; revised August 23, 2018; accepted November 5, 2018. Date of publication November 19, 2018; date of current version December 14, 2018. This work was supported in part by the Israel Science Foundation under Grant 576/16, in part the ISF-NSFC joint research program under Grant 2514/17, and in part MAFAAT-Israel Ministry of Defense. The associate editor coordinating the review of this manuscript and approving it for publication was Dr. Huseyin Hacihabiboglu. *(Corresponding author: Yaakov Buchris.)*

Y. Buchris, A. Amar, and I. Cohen are with the Department of Electrical Engineering, Technion Israel Institute of Technology, Haifa 32000, Israel (e-mail: sbucris@gmail.com; aamar@technion.ac.il; icohen@ee.technion.ac.il).

J. Benesty is with the INRS-EMT, Universite du Quebec, Montreal, QC H5A 1K6, Canada, also with the Technion Israel Institute of Technology, Haifa 32000, Israel, and also with Aalborg University, Aalborg 9100, Denmark (e-mail: benesty@emt.inrs.ca).

Digital Object Identifier 10.1109/TASLP.2018.2881536

constraints. One of the imposed constraints is a joint-sparsity constraint [46] aimed to ensure that the chosen sensors are joint for all frequency bins in the relevant bandwidth. In other words, the same sensors are used to build the beamformers coefficient vectors in all frequency bins. As the optimization of sensors positions and beamformer coefficients is performed simultaneously over all frequency bins in the relevant bandwidth, we may refer to this design approach as a coherent sparse design. While good results were reported, this method is limited when the number of candidate sensors is an order of magnitude of hundreds or more.

In this paper, we propose a new incoherent sparse array design for nearly FI beamforming. The main idea is to split an ℓ_1-optimization problem with a large number of constraints like in the coherent approach, into several smaller optimization subproblems, each matched to a different frequency bin with a smaller number of constraints. In the first step, an ℓ_1-norm constrained optimization problem is solved for each frequency bin separately, yielding a sparse vector containing the indices of the optimal sensors. All these sparse vectors are then arranged in a matrix, on which the principal component analysis (PCA) algorithm is applied to reduce its dimension. The reduced set of data is then clustered in the third step which determines the joint sparse vector containing the dominant sensors positions, i.e., the chosen sensors are common to all frequency bins in the bandwidth of interest. The chosen sensors are used in the synthesis step to obtain the FI joint sparse beampattern. As the ℓ_1-norm optimization is performed for each frequency bin separately, we may refer to this approach as the incoherent sparse design. We also present a modified version of the coherent approach [45], which is compared to the proposed incoherent design later in the simulation section. Note that in this paper the terms coherent and incoherent refer to whether or not we optimize the entire bandwidth simultaneously, and have no relation to the phases of the complex frequency-domain beamformer coefficient vectors.

Though the proposed scheme is general, our focus is on superdirective beamformers and DMAs, since we are interested in FI broadband beamformers which also provide high performance level like directivity factor (DF). These families are characterized as small size, dense arrays with high directivity. According to the model of the superdirective beamformers, it is assumed that the element spacing is much smaller than the wavelength of the incoming signal in order to achieve supergain effect [24].

Therefore, in the simulation section, we present two design examples illustrating the benefits of the proposed incoherent sparse design with respect to the coherent one and also to the uniform array design. The first example considers the case of sparse DMAs design with linear geometry, and the second example considers a 2D planar superdirective beamformer. In the first example, both the coherent and the incoherent sparse design approaches obtain similar performance levels but the computation runtime of the incoherent design was shorter by almost two orders of magnitude than that of the coherent design. Also, it is shown that the sparse designs constitute a good compromise between robustness to array imperfections and prevention of grating lobes. For the second example, the coherent design was infeasible using a standard hardware, while the incoherent design was still feasible and maintained the aforementioned advantages with respect to the uniform design approaches. These results demonstrate that the incoherent sparse design is more practical for applications involving large arrays with hundreds of candidate sensors. Moreover, in some applications adaptive versions of the incoherent sparse design may be also of a great interest. In such applications, the potential sensors physically exist on the array but it is desired to adaptively choose a sparse subset of sensors and preserve some system resources like energy, processing time, storage, and more.

II. Signal Model and Problem Formulation

Consider $\mathcal{B}_{\mathrm{d}}(\boldsymbol{\rho})$, where $\boldsymbol{\rho}=(\theta,\phi)$ specifies the azimuth θ and the elevation ϕ, to be a desired far-field FI beampattern in the bandwidth of interest Ω.

We are given an array in the q-dimensional space ($q=1,2,3$ in the case of a linear, planar, or volumetric aperture, respectively) with M possible positions for locating the sensors, where the mth position is denoted by $\mathbf{p}_m, m=1,2,\ldots,M$. In its general form, the beampattern of such an array for the angular frequency ω is defined as

$$\mathcal{B}\left(\mathbf{h}(\omega)\right) = \mathbf{h}^H(\omega)\mathbf{d}\left(\mathbf{k}_\omega\left(\boldsymbol{\rho}\right)\right), \tag{1}$$

where the superscript ^{H} denotes the conjugate-transpose operator,

$$\mathbf{h}(\omega)=\left[H_1(\omega),H_2(\omega),\ldots,H_M(\omega)\right]^T \tag{2}$$

is a vector containing the beamformer complex gains in the frequency ω, and the superscript ^{T} denotes the transpose operator. The vector:

$$\mathbf{k}_\omega\left(\boldsymbol{\rho}\right) = -\frac{\omega}{c}\begin{bmatrix}\cos\theta\sin\phi\\ \sin\theta\sin\phi\\ \cos\phi\end{bmatrix} \tag{3}$$

is the wavenumber vector at frequency ω and direction $\boldsymbol{\rho}$ associated with the $M\times 1$ steering vector

$$\mathbf{d}\left(\mathbf{k}_\omega\left(\boldsymbol{\rho}\right)\right)=\left[e^{-\jmath\mathbf{k}_\omega^T(\boldsymbol{\rho})\mathbf{p}_0},e^{-\jmath\mathbf{k}_\omega^T(\boldsymbol{\rho})\mathbf{p}_1},\ldots,e^{-\jmath\mathbf{k}_\omega^T(\boldsymbol{\rho})\mathbf{p}_M}\right]^T, \tag{4}$$

where $\jmath=\sqrt{-1}$, and c is the waveform's speed.

Assume that we select a subset of $K\ll M$ position candidates $\{\mathbf{p}_{i_k}\}_{k=1}^K$, where $\{i_k\}_{k=1}^K\in[1,2,\ldots,M]$ are their indices, which will determine the K spatio-temporal beampatterns for each frequency $\omega\in\Omega$, that is,

$$\mathcal{B}\left(\mathbf{h}(\omega),\mathbf{T}_{\mathrm{sc}}\left(\mathbf{i}_K\right)\right) = \mathbf{h}^H(\omega)\mathbf{T}_{\mathrm{sc}}^T\left(\mathbf{i}_K\right)\mathbf{T}_{\mathrm{sc}}\left(\mathbf{i}_K\right)\mathbf{d}\left(\mathbf{k}_\omega\left(\boldsymbol{\rho}\right)\right), \tag{5}$$

where $\mathbf{i}_K=[i_1,i_2,\ldots,i_K]^T$ and $\mathbf{T}_{\mathrm{sc}}\left(\mathbf{i}_K\right)$ is a $K\times M$ FI selection matrix, i.e., containing K rows of an $M\times M$ identity matrix corresponding to the indices $\{i_k\}_{k=1}^K$. Note that the following property is satisfied: $\mathbf{T}_{\mathrm{sc}}\left(\mathbf{i}_M\right)=\mathbf{I}_M$ where $\mathbf{i}_M=[1,2,\ldots,M]^T$ and $\mathbf{I}_M$ is the $M\times M$ identity matrix.

Our goal is stated as follows: we want to select a set of K positions out of the M candidate positions such that the

synthesized beampattern $\mathcal{B}\left(\mathbf{h}(\omega), \mathbf{T}_{\mathrm{sc}}\left(\mathbf{i}_K\right)\right), \forall \omega \in \Omega$ will be FI but at the same time will be as close as possible to the desired power beampattern, $\mathcal{B}_{\mathrm{d}}\left(\boldsymbol{\rho}\right)$ (in the mean square error sense), under some design constraints to be specified below.

III. Typical Design Constraints

We now present several design constraints which are supposed to ensure FI broadband beampattern. Given the reference beampattern $\mathcal{B}_{\mathrm{d}}\left(\boldsymbol{\rho}\right)$, we can use the LS error constraint to get the desired FI beampattern, generally defined as

$$\int_{\Omega}\int_{\Theta}\left\|\mathcal{B}_{\mathrm{d}}\left(\boldsymbol{\rho}\right)-\mathbf{h}^{H}\left(\omega\right)\mathbf{d}\left(\mathbf{k}_{\omega}\left(\boldsymbol{\rho}\right)\right)\right\|_2^2 d\omega d\boldsymbol{\rho}\leq\epsilon_{\mathrm{t}}, \tag{6}$$

where Ω and Θ denote the frequency and angle range of interest, respectively, $||\cdot||_2$ is the ℓ_2-norm, and ϵ_{t} is a small positive tolerance parameter indicating the total overall allowed error. Despite its generality, by using (6) directly we cannot take into consideration that there is a difference in the ability to obtain FI beampattern in different frequencies and also that there are spatial regions that are more important than others, e.g., the mainlobe region is more important than the sidelobe regions. Therefore, we uniformly discretize both the frequency and angle spaces and introduce J frequency bins $\{\omega_j\}_{j=1}^{J}\in\Omega$, and P directions $\left\{\boldsymbol{\rho}_p\right\}_{p=1}^{P}\in\Theta$ that cover the entire beampattern. We set L out of the P directions that cover the mainlobe region Θ_{m}, and define $\boldsymbol{K}_j^{\mathrm{m}}$ to be the set containing these directions on frequency ω_j, i.e.,

$$\boldsymbol{K}_j^{\mathrm{m}}=\left\{\mathbf{k}_{\omega_j}\left(\boldsymbol{\rho}_1\right),\mathbf{k}_{\omega_j}\left(\boldsymbol{\rho}_2\right),\ldots,\mathbf{k}_{\omega_j}\left(\boldsymbol{\rho}_L\right)\right\}, \tag{7}$$

where the superscript m stands for mainlobe. Similarly, we define the set $\boldsymbol{K}_j^{\mathrm{s}}$ containing $P-L$ directions that cover the sidelobe region Θ_{s} as

$$\boldsymbol{K}_j^{\mathrm{s}}=\left\{\mathbf{k}_{\omega_j}\left(\boldsymbol{\rho}_{L+1}\right),\mathbf{k}_{\omega_j}\left(\boldsymbol{\rho}_{L+2}\right),\ldots,\mathbf{k}_{\omega_j}\left(\boldsymbol{\rho}_P\right)\right\}, \tag{8}$$

where the superscript s stands for sidelobe.

We can reformulate (6) as

$$\begin{aligned}
&\int_{\Omega}\int_{\Theta}\left\|\mathcal{B}_{\mathrm{d}}\left(\boldsymbol{\rho}\right)-\mathbf{h}^{H}\left(\omega\right)\mathbf{d}\left(\mathbf{k}_{\omega}\left(\boldsymbol{\rho}\right)\right)\right\|_2^2 d\omega d\boldsymbol{\rho}\\
&\approx C\sum_{\omega_j\in\Omega}\sum_{\boldsymbol{\rho}_p\in\Theta_{\mathrm{m}}}\left\|\mathcal{B}_{\mathrm{d}}\left(\boldsymbol{\rho}\right)-\mathbf{h}^{H}\left(\omega_j\right)\mathbf{d}\left(\mathbf{k}_{\omega_j}\left(\boldsymbol{\rho}_p\right)\right)\right\|_2^2\\
&\quad+C\sum_{\omega_j\in\Omega}\sum_{\boldsymbol{\rho}_p\in\Theta_{\mathrm{s}}}\left\|\mathcal{B}_{\mathrm{d}}\left(\boldsymbol{\rho}\right)-\mathbf{h}^{H}\left(\omega_j\right)\mathbf{d}\left(\mathbf{k}_{\omega_j}\left(\boldsymbol{\rho}_p\right)\right)\right\|_2^2 \qquad (9)\\
&=C\sum_{\omega_j\in\Omega}\left\|\left(\mathbf{b}_{\mathrm{d}}^{\mathrm{m}}\right)^{T}-\mathbf{h}^{H}\left(\omega_j\right)\mathbf{T}_{\mathrm{s}}^{T}\left(\mathbf{i}_K\right)\mathbf{T}_{\mathrm{s}}\left(\mathbf{i}_K\right)\mathbf{D}\left(\boldsymbol{K}_j^{\mathrm{m}}\right)\right\|_2^2\\
&\quad+C\sum_{\omega_j\in\Omega}\left\|\left(\mathbf{b}_{\mathrm{d}}^{\mathrm{s}}\right)^{T}-\mathbf{h}^{H}\left(\omega_j\right)\mathbf{T}_{\mathrm{s}}^{T}\left(\mathbf{i}_K\right)\mathbf{T}_{\mathrm{s}}\left(\mathbf{i}_K\right)\mathbf{D}\left(\boldsymbol{K}_j^{\mathrm{s}}\right)\right\|_2^2,
\end{aligned}$$

where C is a positive constant representing the contribution of the differential $d\omega d\boldsymbol{\rho}$,

$$\mathbf{D}\left(\boldsymbol{K}_j^{\mathrm{m}}\right)=\left[\mathbf{d}\left(\mathbf{k}_{\omega_j}\left(\boldsymbol{\rho}_1\right)\right),\mathbf{d}\left(\mathbf{k}_{\omega_j}\left(\boldsymbol{\rho}_2\right)\right),\ldots,\mathbf{d}\left(\mathbf{k}_{\omega_j}\left(\boldsymbol{\rho}_L\right)\right)\right] \tag{10}$$

is an $M\times L$ matrix, and

$$\mathbf{b}_{\mathrm{d}}^{\mathrm{m}}=\left[\mathcal{B}_{\mathrm{d}}\left(\boldsymbol{\rho}_1\right),\mathcal{B}_{\mathrm{d}}\left(\boldsymbol{\rho}_2\right),\ldots,\mathcal{B}_{\mathrm{d}}\left(\boldsymbol{\rho}_L\right)\right]^{T} \tag{11}$$

is a vector containing the desired beampattern in the directions covering the mainlobe. The matrix $\mathbf{D}\left(\boldsymbol{K}_j^{\mathrm{s}}\right)$ is defined similarly to $\mathbf{D}\left(\boldsymbol{K}_j^{\mathrm{m}}\right)$, and the vector $\mathbf{b}_{\mathrm{d}}^{\mathrm{s}}$ is defined similarly to $\mathbf{b}_{\mathrm{d}}^{\mathrm{m}}$.

As a mainlobe constraint we can decompose the first summation term of (9) into multiple joint-sparse constraints, that is, $\forall\omega_j\in\Omega$,

$$\mathcal{C}_1:\left\|\left(\mathbf{b}_{\mathrm{d}}^{\mathrm{m}}\right)^{T}-\mathbf{h}^{H}\left(\omega_j\right)\mathbf{T}_{\mathrm{s}}^{T}\left(\mathbf{i}_K\right)\mathbf{T}_{\mathrm{s}}\left(\mathbf{i}_K\right)\mathbf{D}\left(\boldsymbol{K}_j^{\mathrm{m}}\right)\right\|_2^2\leq\epsilon_1(\omega_j), \tag{12}$$

where $\epsilon_1(\omega_j)$ is a small positive parameter.

Similarly, for the sidelobe constraint we can decompose the second summation term in (9) into multiple joint-sparse constraints, and write $\forall\omega_j\in\Omega$,

$$\mathcal{C}_2:\left\|\left(\mathbf{b}_{\mathrm{d}}^{\mathrm{s}}\right)^{T}-\mathbf{h}^{H}\left(\omega_j\right)\mathbf{T}_{\mathrm{s}}^{T}\left(\mathbf{i}_K\right)\mathbf{T}_{\mathrm{s}}\left(\mathbf{i}_K\right)\mathbf{D}\left(\boldsymbol{K}_j^{\mathrm{s}}\right)\right\|_2^2\leq\epsilon_2(\omega_j), \tag{13}$$

where $\epsilon_2(\omega_j)$ is a small positive parameter. Typically, $\epsilon_1(\omega_j)<\epsilon_2(\omega_j)$ since the mainlobe region has more influence on the performance than the sidelobe region. Note that both $\epsilon_1(\omega_j)$ and $\epsilon_2(\omega_j)$ are frequency-varying parameters as the capability to satisfy either $\mathcal{C}_1$ or $\mathcal{C}_2$ in adequate accuracy depends on frequency. We can also establish the following relationship:

$$C\sum_{\omega_j\in\Omega}\epsilon_1(\omega_j)+C\sum_{\omega_j\in\Omega}\epsilon_2(\omega_j)\leq\epsilon_{\mathrm{t}}. \tag{14}$$

Clearly, imposing only $\mathcal{C}_1$ and $\mathcal{C}_2$ does not ensure that the array responses $\mathcal{B}\left(\mathbf{h}(\omega_j),\mathbf{T}_{\mathrm{s}}\left(\mathbf{i}_K\right)\right),\omega_j\in\Omega$ will not distort the signal of interest and especially that they will be robust to array calibration and model mismatch errors. Hence, we include two more constraints. The first is the common distortionless response, stating that, $\forall\omega_j\in\Omega$,

$$\mathcal{C}_3:\mathbf{h}^{H}\left(\omega_j\right)\mathbf{T}_{\mathrm{s}}^{T}\left(\mathbf{i}_K\right)\mathbf{T}_{\mathrm{s}}\left(\mathbf{i}_K\right)\mathbf{d}\left(\mathbf{k}_{\omega_j}\left(\boldsymbol{\rho}_{\mathrm{s}}\right)\right)=1, \tag{15}$$

where $\mathbf{k}_{\omega_j}\left(\boldsymbol{\rho}_{\mathrm{s}}\right)$ is the wavenumber of the desired signal at frequency ω_j and direction $\boldsymbol{\rho}_{\mathrm{s}}$. The second is the limitation of the white noise output power, given as, $\forall\omega_j\in\Omega$,

$$\mathcal{C}_4:\mathbf{h}^{H}\left(\omega_j\right)\mathbf{T}_{\mathrm{s}}^{T}\left(\mathbf{i}_K\right)\mathbf{T}_{\mathrm{s}}\left(\mathbf{i}_K\right)\mathbf{h}\left(\omega_j\right)\leq\gamma(\omega_j), \tag{16}$$

where $\gamma(\omega_j)$ is a parameter expressing the maximal allowed white noise output power at frequency ω_j. Note that due to the distortionless constraint specified by (15), the formulation of (16) is equivalent to restricting the white noise gain (WNG) of the array to be above a certain threshold value [47, ch.6]. The WNG, given by [17],

$$\mathcal{W}\left(\mathbf{h}(\omega_j)\right)=\frac{\left|\mathbf{h}^{H}\left(\omega_j\right)\mathbf{d}\left(\mathbf{k}_{\omega_j}\left(\boldsymbol{\rho}\right)\right)\right|^2}{\mathbf{h}^{H}\left(\omega_j\right)\mathbf{h}\left(\omega_j\right)}, \tag{17}$$

is a measure indicating the array gain in the presence of uncorrelated white noise. It also indicates the sensitivity of the array to model mismatch errors [47].

Combining constraints $\mathcal{C}_1, \mathcal{C}_2, \mathcal{C}_3, \mathcal{C}_4$, we can formulate the general joint-sparse problem of interest as

$$\begin{aligned} &\text{minimize} \quad \{\text{number of active sensors} - K\} \\ &\text{subject to} \quad \mathcal{C}_1, \mathcal{C}_2, \mathcal{C}_3, \mathcal{C}_4, \forall \omega_j \in \Omega, \end{aligned} \tag{18}$$

whose solution yields the jointly-sparse filters

$$\mathbf{h}_K(\omega_j) = \mathbf{T}_{\mathrm{s}}(\mathbf{i}_K)\,\mathbf{h}(\omega_j), \forall \omega_j \in \Omega. \tag{19}$$

In this work, we propose two approaches to practically solve (18). The first approach, referred to as the coherent approach, is a modified version of what have been presented in [45]. Accordingly, the joint-sparse filters $\{\mathbf{h}_K(\omega_j)\}_{j=1}^J$ are obtained by a direct ℓ_1-norm optimization over all frequencies and directions of interest, simultaneously. We propose a second approach, where the ℓ_1-norm optimization is performed for each frequency bin $\omega_j \in \Omega$ separately, and based on these selections the joint-sparse sensors are determined. We refer to that proposed approach as the incoherent approach. The advantage of the proposed incoherent approach over the coherent approach is by its reduced computationally which makes the incoherent approach more feasible for practical designs, especially where the number of potential sensors is an order of hundreds.

It is worth noting that both the coherent and the incoherent approaches can be used for either an offline or an online design. In the offline case, once the K chosen sensors are already determined, the corresponding array is constructed using only these sensors. In the online case, all the M candidate sensors physically exist on the array, and a sparse subset of K sensors are adaptively chosen, which are joint to all the frequencies in the relevant bandwidth. We do not consider here the case where different subsets of K sensors are adaptively chosen for each frequency bin. We now describe in details both these approaches.

IV. Coherent Design of FI Sparse Arrays

This approach provides the K sensors by direct optimization over all frequencies. Theoretically, sparse solutions can be obtained by minimizing the ℓ_0-norm of the vector, which is, however, an NP-hard combinatorial optimization problem. A practical alternative is to solve an ℓ_1-norm optimization problem instead [48]. Our problem is more complicated since another essential constraint should be imposed. This is the joint-sparsity constraint which insures that all the filters $\{\mathbf{h}_K(\omega_j)\}_{j=1}^J$ have the same sparse pattern, i.e., the sensors positions which are chosen out of all the potential positions are common over all the frequencies in the signal's bandwidth of interest Ω. The way to insert such a constraint is by minimizing the ℓ_{12}-norm instead of the ℓ_1-norm [49]. It is defined as the following: suppose we have the vectors $\mathbf{x}_i, i = 1, 2, \ldots, n$, of length M, and define $\mathbf{X} = [\mathbf{x}_1, \mathbf{x}_2, \ldots, \mathbf{x}_n]$ to be a matrix containing these vectors in its columns, then the ℓ_{12}-norm of the matrix $\mathbf{X}$ is defined as [46]

$$\|\mathbf{X}\|_{12} \triangleq \sum_{m=1}^{M} \left(\sum_{i=1}^{n} |\mathbf{X}[m,i]|^2 \right)^{\frac{1}{2}}, \tag{20}$$

where $\mathbf{X}[m,i]$ being the entry corresponds to the mth row and the ith column of $\mathbf{X}$. Herein, we present the optimization problem yielding the required joint-sparse filters. It is a modified version of what have been presented in [45], that is,

$$\begin{aligned} &\underset{\{\mathbf{h}(\omega_j)\}_{j=1}^J}{\text{minimize}} \quad \sum_{m=1}^{M} \alpha_m^k \eta_m \\ &\text{subject to} \quad \eta_m \geq \left\|\bar{\mathbf{h}}_m\right\|_2, \\ &\text{and} \ \ \forall \omega_j \in \Omega \\ &\qquad \mathbf{h}^H(\omega_j)\,\mathbf{d}\left(\mathbf{k}_{\omega_j}(\boldsymbol{\rho}_{\mathrm{s}})\right) = 1 \\ &\qquad \mathbf{h}^H(\omega_j)\,\mathbf{h}(\omega_j) \leq \gamma(\omega_j) \\ &\qquad \left\|(\mathbf{b}_{\mathrm{d}}^{\mathrm{m}})^T - \mathbf{h}^H(\omega_j)\,\mathbf{D}\left(\mathbf{K}_j^{\mathrm{m}}\right)\right\|_2^2 \leq \epsilon_1(\omega_j) \\ &\qquad \left\|(\mathbf{b}_{\mathrm{d}}^{\mathrm{s}})^T - \mathbf{h}^H(\omega_j)\,\mathbf{D}\left(\mathbf{K}_j^{\mathrm{s}}\right)\right\|_2^2 \leq \epsilon_2(\omega_j), \end{aligned} \tag{21}$$

where

$$\begin{aligned} \bar{\mathbf{h}}_m &= [H_m(\omega_1), H_m(\omega_2), \ldots, H_m(\omega_J)]^T, \\ m &= 1, 2, \ldots, M, \end{aligned} \tag{22}$$

$\alpha_m^k = 1/\left(\eta_m^{k-1} + \epsilon\right)$ for $k > 1$ and $\alpha_m^1 = 1$, η_m^{k-1} is the result obtained from the $(k-1)$th iteration, and ϵ is a regularization parameter. We run this algorithm iteratively until

$$\Delta\boldsymbol{\eta} \triangleq \frac{\left\|\boldsymbol{\eta}^k - \boldsymbol{\eta}^{k-1}\right\|_2}{\|\boldsymbol{\eta}^k\|_2} \leq \epsilon_\eta, \tag{23}$$

where $\boldsymbol{\eta}^k = \left[\eta_1^k, \eta_2^k, ..., \eta_M^k\right]^T$, and ϵ_η is a small positive parameter. This iterative algorithm yields a sparse solution which is a good approximation to the ℓ_0-norm solution. As the optimization problem in (21) is convex, it can be solved by convex optimization methods (e.g., CVX toolbox [50]).

Both the vectors $\boldsymbol{\eta}^k$ and $\{\mathbf{h}(\omega_j)\}_{j=1}^J$ are iteratively updated using (21) until (23) is satisfied. The K sensors corresponding to the K largest entries of the vector $\boldsymbol{\eta}^k$ will determine the support S of the filters $\{\mathbf{h}(\omega_j)\}_{j=1}^J$, from which the desired sparse filters $\{\mathbf{h}_K(\omega_j)\}_{j=1}^J$ satisfying $\mathcal{C}_1, \mathcal{C}_2, \mathcal{C}_3, \mathcal{C}_4$ are obtained.

V. Incoherent Design of FI Sparse Arrays

In the previous section, the optimization problem in (21) is solved over the entire bandwidth. It may be very inefficient and sometimes infeasible when a large number of candidate sensors is assumed. In this section, we propose a four-step algorithm which separates between the analysis step of determining the support S of the filters $\{\mathbf{h}(\omega_j)\}_{j=1}^J$ and the synthesis step where the actual filters, $\{\mathbf{h}_K(\omega_j)\}_{j=1}^J$, are calculated. This separation enables to solve the optimization problem much more efficiently and also facilitates design of arrays with a large number of candidate sensors.

Note that the parameter K can be determined in the coherent design from (23). However, in the incoherent design it is not trivial and less intuitive to determine analytically the value of K. In this work, we do not address this problem, and solve a slightly

different problem from what has been defined in (18), assuming that K is given but satisfies $K \ll M$. In the simulations, we may take the same value obtained by the coherent approach, in order to concentrate on the comparison between the incoherent and coherent design. Yet, a method for determining the optimal parameter K for the incoherent design is an important problem to be addressed in a future research. Practically, K can be determined by a line search over this parameter. Later, in the simulation section we present the performance of the incoherent design for different values of K. In the following subsections, we describe each of these steps.

A. Analysis

As a first step, we would like to solve separately $\forall \omega_j \in \Omega$ the following ℓ_1-norm optimization problem:

$$\underset{\mathbf{h}(\omega_j)}{\text{minimize}} \quad \sum_{m=1}^{M} \left| H_m\left(\omega_j\right) \right|$$

subject to

$$\begin{aligned} &\mathbf{h}^H\left(\omega_j\right) \mathbf{d}\left(\mathbf{k}_{\omega_j}\left(\boldsymbol{\rho}_{\mathrm{s}}\right)\right) = 1 \\ &\mathbf{h}^H\left(\omega_j\right) \mathbf{h}\left(\omega_j\right) \leq \gamma(\omega_j) \\ &\left\| \left(\mathbf{b}_{\mathrm{d}}^{\mathrm{m}}\right)^T - \mathbf{h}^H\left(\omega_j\right) \mathbf{D}\left(\mathbf{K}_j^{\mathrm{m}}\right) \right\|_2^2 \leq \epsilon_1(\omega_j) \\ &\left\| \left(\mathbf{b}_{\mathrm{d}}^{\mathrm{s}}\right)^T - \mathbf{h}^H\left(\omega_j\right) \mathbf{D}\left(\mathbf{K}_j^{\mathrm{s}}\right) \right\|_2^2 \leq \epsilon_2(\omega_j). \end{aligned} \tag{24}$$

Similarly to the coherent optimization approach, both the objective function and the constraints in (24) are convex, therefore, (24) can be solved by convex optimization methods (e.g., using CVX toolbox [50]).

We solve (24) $\forall \omega_j \in \Omega$ separately, and get the sparse vectors, $\mathbf{h}_{\mathrm{A}}\left(\omega_j\right), j = 1, 2, \ldots, J$ of length M, where the subscript A stands for analysis. Each of these vectors has different support which influenced by the frequency. Specifically, as the frequency increases, the support becomes smaller. Let us define the data matrix $\mathbf{H}_{\mathrm{A}}$ of size $M \times J$ containing the vectors $\{\mathbf{h}_{\mathrm{A}}(\omega_j)\}_{j=1}^{J}$ in its columns, i.e.,

$$\mathbf{H}_{\mathrm{A}} = \left[\mathbf{h}_{\mathrm{A}}(\omega_1), \mathbf{h}_{\mathrm{A}}(\omega_2), \ldots, \mathbf{h}_{\mathrm{A}}(\omega_J)\right]. \tag{25}$$

Similarly to the coherent approach where the solution for (21) yields K sensors jointly used for all the frequencies, we would like also for the incoherent approach to make an elegant decision regarding the best choice of K sensors jointly used during the array synthesis process.

The problem of determining the K most dominant sensors positions where K is given, can be viewed as a clustering problem whose solution may yield K clusters of sensors. Therefore, we treat the matrix $\mathbf{H}_{\mathrm{A}}$ as a measurements matrix of M observations, each with J features. In other words, each of the M potential microphones is represented by a feature vector in $\mathbb{C}^J$.

B. Dimensionality Reduction

As the matrix $\mathbf{H}_{\mathrm{A}}$ was obtained by an ℓ_1-norm optimization, it consists of the sparse vectors $\{\mathbf{h}_{\mathrm{A}}(\omega_j)\}_{j=1}^{J}$ in its columns,

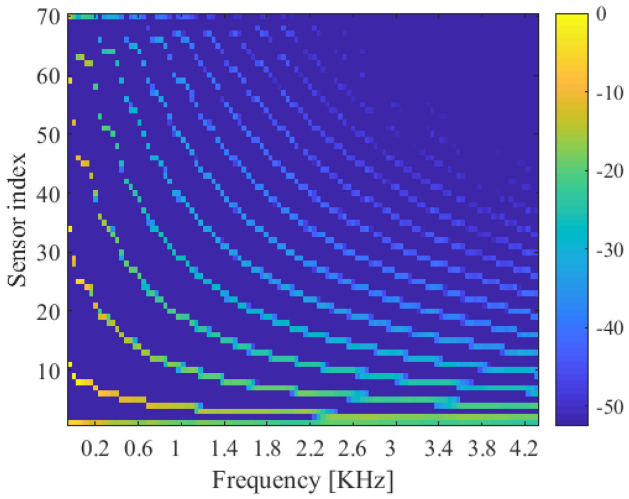

Fig. 1. Absolute values of the elements of the matrix $\mathbf{H}_{\mathrm{A}}$ on a logarithmic scale.

and thus effectively a rank-deficient matrix with a decaying singular values spectrum. Fig. 1 presents a typical example of the absolute value of $\mathbf{H}_{\mathrm{A}}$ on a logarithmic scale. The parameters for this example are specified later in Section VII-A. One can see that this matrix is sparse: For each frequency five to ten sensors are required. Furthermore, as the frequency increases, the energy of the selected sensors is spread over a smaller array aperture. This structure stems from the fact that in each frequency the spatial sampling constraint should be satisfied, meaning that the element spacing should be smaller than half the wavelength at that frequency.

In order to show that $\mathbf{H}_{\mathrm{A}}$ is indeed effectively a rank-deficient matrix, we may look at the sampled correlation matrix of $\mathbf{H}_{\mathrm{A}}$:

$$\mathbf{R}_{\mathrm{A}} = \mathbf{H}_{\mathrm{A}}^H \mathbf{H}_{\mathrm{A}} \tag{26}$$

of size $J \times J$.

The jth diagonal element of $\mathbf{R}_{\mathrm{A}}$ is simply the squared-norm of the filter vector $\mathbf{h}_{\mathrm{A}}(\omega_j)$. As the frequency increases, the coefficient energy of a superdirective beamformer usually decreases, as can be seen in Fig. 1. Due to the sparseness of the matrix $\mathbf{H}_{\mathrm{A}}$ the off-diagonal entries of $\mathbf{R}_{\mathrm{A}}$ are very close to zero since two different columns of $\mathbf{H}_{\mathrm{A}}$ are uncorrelated. These considerations lead to a conclusion that $\mathbf{R}_{\mathrm{A}}$ is effectively a rank-deficient matrix as observed from Fig. 2 where the absolute value of $\mathbf{R}_{\mathrm{A}}$ on a logarithmic scale is presented.

The effective low rank of the matrix $\mathbf{R}_{\mathrm{A}}$, which results in a decaying eigenvalues spectrum as will be shown later, implies also the same property for the matrix $\mathbf{H}_{\mathrm{A}}$, because of the well-known relation between the singular values of both matrices: Let $\{\sigma_i\}_{i=1}^{r}$ be the singular values of the matrix $\mathbf{H}_{\mathrm{A}}$ where r denotes its rank, then $\left\{\lambda_i = \sigma_i^2\right\}_{i=1}^{r}$ are the eigenvalues of the matrix $\mathbf{R}_{\mathrm{A}}$.

Therefore, we may assume that the matrix $\mathbf{H}_{\mathrm{A}}$ contains some redundancy, as its high dimensional feature vectors are not spread across the entire space, but rather concentrated on a significantly lower dimension. Thus, prior to the clustering step, we apply a pre-processing step of dimensionality reduction to the

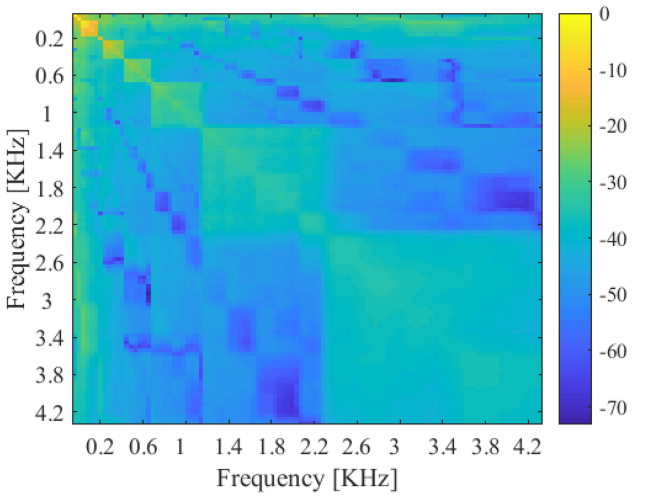

Fig. 2. Absolute values of the elements of the matrix $\mathbf{R}_{\mathrm{A}}$ on a logarithmic scale.

matrix $\mathbf{H}_{\mathrm{A}}$. In this work, we use the principal component analysis (PCA) algorithm [51] commonly used for dimensionally reduction, which is a linear algorithm. Of course, other linear and non-linear dimension reduction techniques can be used and are part of a future research.

The input to the PCA algorithm is the data matrix $\mathbf{H}_{\mathrm{A}}$ of size $M \times J$ defined above. Define the matrix $\overline{\mathbf{H}}_{\mathrm{A}}$ to be a centralized version of $\mathbf{H}_{\mathrm{A}}$, i.e., the sampled mean of each column of $\mathbf{H}_{\mathrm{A}}$ has been shifted to zero. The output of the PCA algorithm yields the compact data representation matrix:

$$\mathbf{H}_{\mathrm{R}} = \overline{\mathbf{H}}_{\mathrm{A}}\,\overline{\mathbf{U}}, \tag{27}$$

where $\overline{\mathbf{U}}$ is a matrix of size $J \times i$ contains i eigenvectors corresponding to the i largest eigenvalues, and the subscript R stands for reduced.

The column dimension i of the matrix $\overline{\mathbf{U}}$ is set according to the following criteria: let $\lambda_1 \geq \lambda_2 \geq \cdots \geq \lambda_J$ be the eigenvalues of the matrix $\mathbf{R}_{\mathrm{A}}$, then we choose the first $i \ll J$ eigenvalues which satisfy

$$\Sigma_i \triangleq \frac{\sum_{j=1}^{i} \lambda_j}{\sum_{j=1}^{J} \lambda_j} \leq \alpha, \tag{28}$$

where typically $0.6 \leq \alpha \leq 0.9$.

C. Clustering

The next step is to apply a clustering algorithm on the rows of $\mathbf{H}_{\mathrm{R}}$ in order to determine the most dominant microphones. Herein, we use the k-means algorithm [52] to divide all the M sensors into K clusters. The k-means algorithm is a two-step iterative algorithm, where in each iteration the first step is to assign each observation to the cluster whose mean yields the least within-cluster sum of squares. Then, an update step is applied where updated mean values are calculated to be the centroids of the observations in the new clusters. The algorithm also includes an initialization step by choosing a set of K mean values. The k-means algorithm is heuristic, and convergence to the global minimum is not assured, meaning that the result may depend on the initial clusters. Therefore, it is common to run it multiple times (typically 10–20 times) with different initial conditions, and choose the best solution, i.e., the one that yields the minimal within-cluster sums of points-to-centroid distances. Finally, we choose one representative microphone from each of the K chosen clusters, which is closest to the corresponding centroid. We denote by $\{\mathbf{p}_{i_k}\}_{k=1}^{K}$ the positions of the chosen sensors.

Note that in this work we employ separately a dimensionally reduction based PCA stage and a clustering k-means based stage. A different approach that combines both these stages together is presented in [53]. Considering such an approach for the selection of the K candidate sensors is a subject for a future research.

D. Synthesis

In Section V-A the goal is to determine the minimal number of the active sensors, K, which fulfill the constraints, and consequently, the objective function was the ℓ_1-norm of the filters $\{\mathbf{h}(\omega_j)\}_{j=1}^{J}$. In the synthesis step, where the K indices $\{i_k\}_{k=1}^{K}$ of the sensors used to build the FI beampattern are already determined, there is no need to solve an ℓ_1-norm optimization problem and instead we may solve an optimization problem whose objective function is related to the four $\mathcal{C}_1, \mathcal{C}_2, \mathcal{C}_3, \mathcal{C}_4$ constraints presented in Section III. A reasonable choice is to minimize the noise output power (i.e., $\mathcal{C}_4$), subject to the remaining constraints, $\mathcal{C}_1, \mathcal{C}_2$, and $\mathcal{C}_3$. Therefore, we can formulate it as follows: $\forall \omega_j \in \Omega$, solve

$$\underset{\mathbf{h}_K(\omega_j)}{\text{minimize}} \quad \left\|\mathbf{h}_K^H(\omega_j)\right\|_2^2$$

subject to

$$\begin{aligned} &\mathbf{h}_K^H(\omega_j)\,\mathbf{d}_K\left(\mathbf{k}_{\omega_j}(\boldsymbol{\rho}_{\mathrm{s}})\right) = 1 \\ &\left\|(\mathbf{b}_{\mathrm{d}}^{\mathrm{m}})^T - \mathbf{h}_K^H(\omega_j)\,\mathbf{D}_K\left(\mathbf{K}_j^{\mathrm{m}}\right)\right\|_2^2 \leq \epsilon_1(\omega_j) \\ &\left\|(\mathbf{b}_{\mathrm{d}}^{\mathrm{s}})^T - \mathbf{h}_K^H(\omega_j)\,\mathbf{D}_K\left(\mathbf{K}_j^{\mathrm{s}}\right)\right\|_2^2 \leq \epsilon_2(\omega_j), \end{aligned} \tag{29}$$

where $\mathbf{d}_K\left(\mathbf{k}_{\omega_j}(\boldsymbol{\rho}_{\mathrm{s}})\right) = \mathbf{T}_{\mathrm{s}}(\mathbf{i}_K)\,\mathbf{d}\left(\mathbf{k}_{\omega_j}(\boldsymbol{\rho}_{\mathrm{s}})\right)$, $\mathbf{D}_K\left(\boldsymbol{K}_j^{\mathrm{m}}\right) = \mathbf{T}_{\mathrm{s}}(\mathbf{i}_K)\,\mathbf{D}\left(\boldsymbol{K}_j^{\mathrm{m}}\right)$, and $\mathbf{D}_K\left(\boldsymbol{K}_j^{\mathrm{s}}\right) = \mathbf{T}_{\mathrm{s}}(\mathbf{i}_K)\,\mathbf{D}\left(\boldsymbol{K}_j^{\mathrm{s}}\right)$. The resulting filters $\{\mathbf{h}_K(\omega_j)\}_{j=1}^{J}$ correspond to the sensors located in the indices $\{\mathbf{p}_{i_k}\}_{k=1}^{K}$. This fact is important since it means that we can use only K out of M sensors and still obtain adequate results as presented later in the simulations section.

VI. Parameters Adjustment

In both the coherent and incoherent approaches several parameters must be chosen properly in order to get optimal performance. While for the incoherent approach a simple procedure to initialize these parameters will be offered in the following, for the coherent approach, searching for the appropriate parameters may be a much more exhaustive task as it should be done over all the frequency bins, simultaneously. Therefore, we may concentrate on the incoherent design.

The most important parameters to be determined are the number of active sensors, K, and the tolerance parameters $\{\epsilon_1(\omega_j)\}_{j=1}^{J}$, $\{\epsilon_2(\omega_j)\}_{j=1}^{J}$, and $\{\gamma(\omega_j)\}_{j=1}^{J}$. Other parameters

like ϵ and ϵ_η are set once, and are not changed with frequency. We propose the following procedure for the initialization and adjustment of these parameters.

As noted before, determining the number of active sensors, K, is an open question, and we assume it is given. In the next section, an example illustrating the influence of this parameter on the performance is presented. Practically, a very rough line search over K will be sufficient to get a reasonable value for this parameter. In the next section, we use the same value obtained by the coherent approach for comparison.

In order to determine properly initial values for the tolerance parameters $\{\epsilon_1(\omega_j)\}_{j=1}^J$, $\{\epsilon_2(\omega_j)\}_{j=1}^J$, and $\{\gamma(\omega_j)\}_{j=1}^J$, we may conduct a two-dimensional grid search of $\epsilon_1(\omega_1)$ and $\gamma(\omega_1)$. We set $\epsilon_2(\omega_1) = \beta\epsilon_1(\omega_1)$, where $\beta > 1$ is fixed and not changed at all. We set a uniform grid for possible values of $\{\epsilon_1(\omega_j)\}_{j=1}^J$ and $\{\gamma(\omega_j)\}_{j=1}^J$. In some cases, like the one presented in Section VII-A, $\{\gamma(\omega_j)\}_{j=1}^J$ can be modeled and bounded by lower and upper limits corresponding to the worst case and the best case of output noise power. In these cases, we may apply a grid of possible values between the worst case and the best case.

The above two-dimensional search provides the optimal set of parameters $\{\epsilon_1(\omega_1), \epsilon_2(\omega_1), \gamma(\omega_1)\}$. We use this set for the next frequency bins where in each one we adaptively increase $\epsilon_1(\omega_j)$ and $\epsilon_2(\omega_j)$ by a factor of g_1 each time the CVX solver do not yield a feasible solution to (24), meaning that we increase the maximal allowed tolerance of $\mathcal{C}_1$ and $\mathcal{C}_2$. Once we find appropriate values of $\epsilon_1(\omega_j)$ and $\epsilon_2(\omega_j)$, we decrease $\gamma(\omega_j)$ by a factor of g_2, and solve the optimization problem. If a feasible solution is accepted, then $\gamma(\omega_j)$ is updated to its new value.

The above parameters initialization and adjustment procedure is a part of the analysis step. The obtained values for these parameters may be also suitable for the synthesis step. Yet, fine-tuning of these parameters may still be required because in the synthesis step, we are restricted to use only K sensors. Such a fine-tuning process can be done similarly to the process described above, used for the analysis step.

VII. Numerical Simulations

The proposed incoherent approach is demonstrated for two classes of superdirective beamformers. The first example shows a sparse design of DMAs with a linear geometry, and the second example considers a sparse design of a superdirective beamformer with a planar geometry. The performance of the incoherent sparse design is compared to that of the coherent design presented in Section IV, and also to the performance of a uniform array design.

A. One-Dimensional Array Design

We consider a sparse design of linear DMAs, which refer to arrays that combine closely spaced sensors to respond to the spatial derivatives of the acoustic pressure field. These small-size arrays yield nearly FI beampatterns, and include the well-known superdirective beamformer as a particular case. Due to the linear geometry, the directivity pattern depends only on the azimuth θ and we can treat the case of two-dimensional beampattern where $\phi = 90^\circ$, i.e., the plane where the array is laid. For the 2D case, the FI beampattern of an N th-order DMA is given by [18]

$$\mathcal{B}_N(\theta) = \sum_{n=0}^{N} a_{N,n} \cos^n \theta, \tag{30}$$

where $\{a_{N,n}\}_{n=0}^N$ are real coefficients, and the desired signal arrives from the endfire direction, i.e., from $\theta = 0^\circ$. For this example $\mathcal{B}_N(\theta)$ is considered to be the desired beampattern, i.e., $\mathcal{B}_{\rm d}(\boldsymbol{\rho}) = \mathcal{B}_N(\theta)$. It is also assumed that the element spacing, δ, is much smaller than the wavelength of the incoming signal, i.e,

$$\forall \omega \in \Omega : \delta \ll \lambda = \frac{2\pi c}{\omega} \Rightarrow \delta \ll \frac{2\pi c}{\omega_{\max}}, \tag{31}$$

in order to approximate the spatial differential of the pressure signal, where $\omega_{\max}$ is the angular frequency corresponding to the highest frequency in the bandwidth of interest, Ω, and $c =$ 340 m/sec.

In spite of their benefits, traditional DMAs suffer from noise amplification, especially at low frequencies. For that, we apply a sparse approach for designing robust DMAs with relatively smaller number of sensors.

We compare between four approaches for design of linear arrays. The first one is our proposed incoherent sparse design presented in the previous section. The second is the coherent sparse design presented in Section IV. The third approach is based on minimum-norm design for N th-order DMAs presented in [16], where K closely uniformly spaced microphones were used to obtain a desired directivity pattern. We refer to this approach as the minimum-norm (MN) approach. The fourth design is similar to the third, but with the only difference that the K sensors are spread uniformly over the entire possible aperture of M sensors. We refer to this approach as the minimum-norm extended array (MNE) approach.

We apply the four approaches to designing a FI broadband beampattern for the range of frequencies between $f_{\rm low} =$ 200 Hz and $f_{\rm high} = 4480$ Hz. Assuming a typical duration of $T = 25$ msec for the window analysis used for the corresponding time-domain received signal, the frequency resolution is $\Delta f = 1/T = 40$ Hz. Thus, the number of bins J can be calculated as $J = \frac{f_{\rm high} - f_{\rm low}}{\Delta f} = 108$. For the sparse approaches, an initial array of $M = 70$ potential microphones, with element spacing of $\delta = 1$ cm $\ll \frac{2\pi c}{\omega_{\max}} \approx 7.6$ cm between two adjacent sensors is assumed.

We design a third-order hypercardioid pattern (i.e., $N = 3$) which maximizes the DF, whose theoretical beampattern is given according to (30) as

$$\mathcal{B}_N^{\rm HC}(\theta) = -0.14 - 0.57\cos\theta + 0.57\cos^2\theta + 1.15\cos^3\theta. \tag{32}$$

For this case we set $\boldsymbol{\rho}_L = \theta_L = 60^\circ$, i.e., the mainlobe region in the azimuthal axis is $-60^\circ \le \theta \le 60^\circ$.

For the MN and MNE approaches, we impose three null directions at $\theta_1 = 51^\circ$, $\theta_2 = 103^\circ$, and $\theta_3 = 154^\circ$, according to the theoretical beampattern of a third-order hypercardioid [18], and distortionless constraint at $\theta = 0^\circ$.

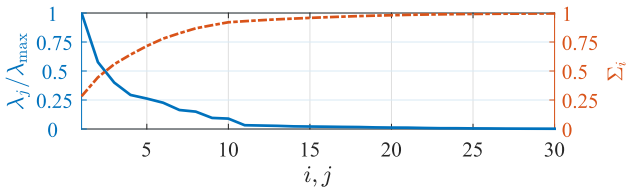

Fig. 3. The spectrum $\lambda_j/\lambda_{\max}, j = 1, 2, ..., J$ of the correlation matrix $\mathbf{R}_{\mathrm{A}}$ (blue solid line), and the quantity Σ_i (28) vs. j (red dashed line) for the third-order asymmetric hypercardioid obtained by the incoherent sparse design.

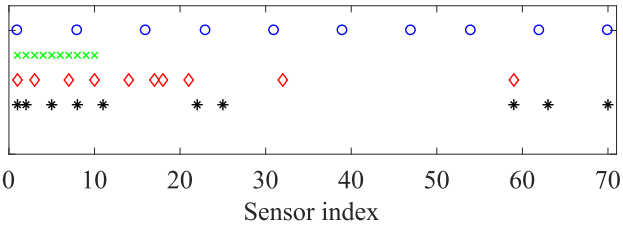

Fig. 4. Array layout for each of the compared design approaches. The black stars line is for the incoherent design. The red diamond line is for the coherent design. The green 'x' line is for the MN approach, and the blue circles line is for the MNE approach.

We set the parameter $\gamma(\omega_j)$ to be

$$\gamma(\omega_j) = \alpha(\omega_j)\gamma_{\mathrm{MN}}(\omega_j) + [1 - \alpha(\omega_j)]\,\gamma_{\mathrm{MNE}}(\omega_j), \qquad (33)$$

where $\gamma_{\mathrm{MN}}(\omega_j) = \mathbf{h}^H_{\mathrm{MN}}(\omega_j)\mathbf{h}_{\mathrm{MN}}(\omega_j)$ is the white noise output power for the case of the MN approach, which yields the maximal white noise output power for the case of K sensors. The other quantity $\gamma_{\mathrm{MNE}}(\omega_j) = \mathbf{h}^H_{\mathrm{MNE}}(\omega_j)\mathbf{h}_{\mathrm{MNE}}(\omega_j)$ is the white noise output power of the MNE approach which yields the lowest white noise output power for the case of K sensors. The frequency-dependent weighting parameter $\alpha(\omega_j)$ is used to get more flexibility in regions where the noise output power is high. As explained in Section VI, a two dimensional grid search is performed in order to find optimal values for $\epsilon_1(\omega_1)$ and $\gamma(\omega_1)$. In this example, we perform a grid of possible values for $\alpha(\omega_1)$, instead. We choose a uniform grid between 0 to 1 with a spacing of 0.1. The meaning of (33) is that we confine the output noise power of the sparse design to a moderate value between the best achievable one and the worst-case value.

In order to build the matrices $\mathbf{D}\left(\boldsymbol{K}^{\mathrm{m}}_j\right)$ and $\mathbf{D}\left(\boldsymbol{K}^{\mathrm{s}}_j\right)$ we uniformly discretize the angular axis with $\Delta\theta = 2^\circ$. We choose the parameters $\epsilon = 10^{-4}$, $\epsilon_\eta = 5 \cdot 10^{-3}$, $\beta = 4$, and $g_1 = g_2 = 1.25$. We set a uniform grid between 0.1 to 2 with a spacing of 0.2 for the line search of $\epsilon_1(\omega_1)$.

For the proposed incoherent approach, we run the first step of analysis presented in Section V-A, with the parameters adjustment procedure presented in Section VI. We get the initial optimal values of $\epsilon_1(\omega_1) = 0.3$, $\epsilon_2(\omega_1) = 1.2$, and $\alpha(\omega_1) = 0.2$. The final values of these parameters were $\epsilon_1(\omega_J) \approx 0.5$, $\epsilon_2(\omega_J) \approx 1.8$, and $\alpha(\omega_J) = 0.4$. We get the $M \times 1$ filter vectors $\mathbf{h}_{\mathrm{A}}(\omega_j), \forall\omega_j \in \Omega$, which are used to construct the matrix $\mathbf{H}_{\mathrm{A}}$ (25) of size $M \times J$, presented in Fig. 1.

We use the matrix $\mathbf{H}_{\mathrm{A}}$ as an input to the PCA algorithm described in Section V-B. In Fig. 3 the eigenvalues of $\mathbf{R}_{\mathrm{A}}$(26) are presented in an ascending order (blue solid line), normalized by the maximal eigenvalue, and also presented is the cumulative function, Σ_i (28) (red dashed line). We observe a rapid decay rate of the eigenvalues which motivates the choice to take a much smaller number of eigenvalues in order to construct the matrix $\mathbf{H}_{\mathrm{R}}$ (27).

The value of $\alpha = 0.6$ in (28) was chosen yielding $i = 3$ (i.e., the first three dominant eigenvalues where selected), as it obtains the best results with respect to other choices of the parameter α. Although non-negligible energy exists also in the remaining eigenvalues, it is expected that only part of them will obtain the optimal results since they may carry most of the variability of the sensors features vectors.

In the next step, we apply the k-means algorithm to the matrix $\mathbf{H}_{\mathrm{R}}$ to obtain K clusters, and in the fourth step, the synthesis was performed using the K sensors according to Section V-D.

We run the coherent approach by solving (21) using the CVX software [50], where we used the optimal values of the tolerance parameters $\{\epsilon_1(\omega_j)\}_{j=1}^J$, $\{\epsilon_2(\omega_j)\}_{j=1}^J$, and $\{\gamma(\omega_j)\}_{j=1}^J$, obtained by the incoherent design. After 7 iterations, we get $\Delta\boldsymbol{\eta} < \epsilon_\eta$ and $K = 10$ dominant sensors were identified, while all the rest are close to zero, meaning that both $\boldsymbol{\eta}$ and the filters $\{\mathbf{h}(\omega_j)\}_{j=1}^J$ are sparse vectors with $K = 10$ active sensors. The number of selected elements remains the same even if more iterations are used. We finally obtain the filters $\{\mathbf{h}_K(\omega_j)\}_{j=1}^J$ using (19).

Fig. 4 presents the array layout for each of the four approaches. The incoherent approach yields the sensors marked by the black stars, while the coherent approach yields the red diamond. One can see that both approaches lead to a similar array layout. Also presented the sensor positions obtained by the MN and MNE approaches, where for these both approaches, the sensors positions are set a-priori. The MN approach achieves the smallest array aperture, yet, it suffers from white noise amplification as will be discussed later.

Fig. 5 illustrates the beampattern (1) of a third-order hypercardioid for a specific frequency of $f = 2500$ Hz, obtained by each of the four approaches (blue dotted line). Also presented is the theoretical beampattern (32) of a third-order hypercardioid (black dashed line). One can see that the MN approach obtains the beampattern which is the most similar to the theoretical value while the MNE has much higher sidelobes due to the spatial aliasing. Both the coherent sparse approach and the incoherent sparse approach obtain beampatterns with similar characteristics.

Fig. 6 shows the WNG (17) and the DF (34) as a function of the frequency obtained by the incoherent sparse design (black dashed line), the coherent sparse design (red circles line), the MNE design (blue triangles line), and the MN design (green diamonds line). Also presented is the theoretical DF of a third-order hypercardioid (magenta stars line). The DF of the array is the gain in signal-to-noise ratio (SNR) for the case of a spherical diffuse noise, i.e., [16]:

$$\mathcal{D}\left(\mathbf{h}(\omega_j)\right) = \frac{\left|\mathbf{h}^H\left(\omega_j\right)\mathbf{d}\left(\mathbf{k}_{\omega_j}\left(\boldsymbol{\rho}\right)\right)\right|^2}{\mathbf{h}^H\left(\omega_j\right)\boldsymbol{\Gamma}_{\mathrm{dn}}\left(\omega_j\right)\mathbf{h}\left(\omega_j\right)}, \qquad (34)$$

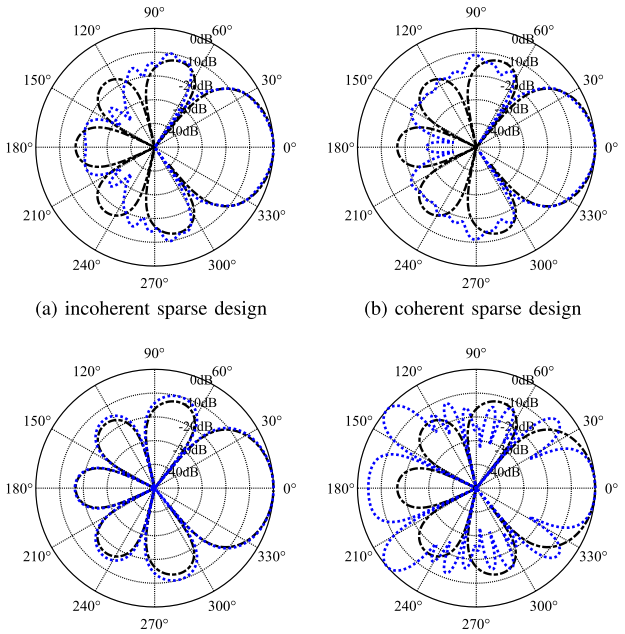

(a) incoherent sparse design (b) coherent sparse design

(c) MN design (d) MNE design

Fig. 5. Beampatterns of a third-order hypercardioid (blue dotted line) for $f = 2500$ Hz, obtained by various approaches. Also presented is the theoretical beampattern of a third-order hypercardioid (black dashed line).

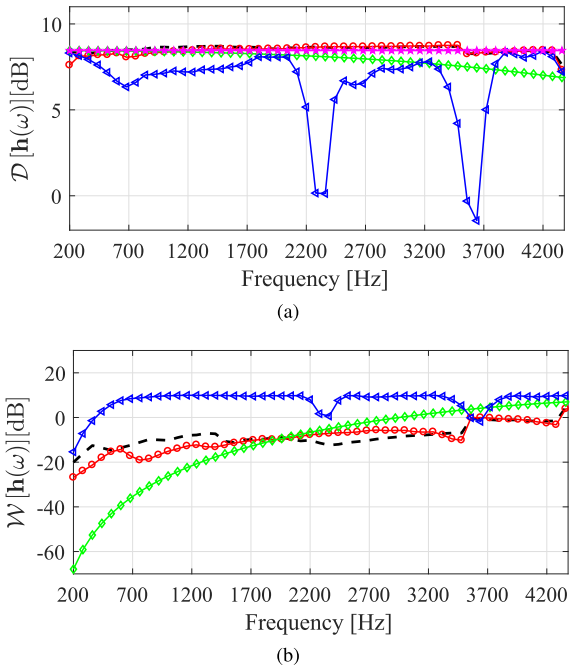

Fig. 6. (a) DF and (b) WNG vs. frequency for the incoherent sparse design (black dashed line), the coherent sparse design (red circles line), the MNE design (blue triangles line), and the MN design (green diamonds line). Also presented is the theoretical DF of a third-order hypercardioid (magenta stars line).

where

$$[\mathbf{\Gamma}_{\mathrm{dn}}(\omega_j)]_{il} = \mathrm{sinc}\left(\frac{\omega_j \delta}{c}(l-i)\right) \tag{35}$$

is an $M \times M$ pseudo-coherence matrix of the diffuse noise field. As expected, both coherent and incoherent sparse approaches obtain similar results in terms of WNG and DF. The main difference is the processing time for each approach. Both approaches were run on an i7-5600U CPU @ 2.6 GHz of INTEL with 12 GB ram. While the incoherent approach takes about 5 minutes of running including the adjustment procedure, the coherent approach run for almost 160 minutes, which is almost two order of magnitudes more than the incoherent approach. Moreover, as written before, we used the values of the tolerance parameters obtained by incoherent approach also for the coherent design. The consequence of adjusting such parameters directly using the coherent design is that such design may take much more time than 160 seconds. Note also that for the coherent approach, an iterative algorithm is required in order to get adequate approximation of ℓ_0-norm. For the incoherent approach, such an iterative algorithm is not required at all, and a good approximation of the ℓ_0-norm is obtained by a single iteration. Yet, both PCA and K-means are iterative algorithms.

The MN obtains nearly FI optimal DF implying on its FI beampattern, but achieves poor WNG, especially for low frequencies, which is a well-known problem of superdirective beamformers in general, and of DMAs in particular. On the contrary, the MNE approach yields superior WNG, but for frequencies above 2000 Hz the DF fluctuates due to the presence of grating lobes, which may appear when $f \geq c/(2\delta_{\mathrm{MNE}})$, where $\delta_{\mathrm{MNE}} = (M-1)\delta/(K-1)$ is the element spacing for the extended uniform array. Substituting the values in this formula we get that for $f \geq 2300$ Hz grating lobes may appear, in accordance with the results presented in this figure.

The synthesized FI beampatterns versus frequency are shown in Fig. 7 for the (a) incoherent approach, (b) the coherent approach, (c) the MN approach, and (d) the MNE approach. This figure reflects the trends inspected by the DF plot. Specifically, for both the coherent and incoherent sparse approaches the beampattern is almost FI, especially in the mainlobe region and less in the sidelobes regions, as dictated by the constraints $\mathcal{C}_1$ and $\mathcal{C}_2$. The MN approach achieves the clearest and most perfect FI beampattern, and in the MNE one can see the grating lobes starting from approximately $f = 2000$ Hz.

As specified before, it is assumed that for the incoherent design, K is given. We now present the influence of this parameter on the performance of the incoherent design. Fig. 8 shows the WNG (17) and the DF (34) as a function of the frequency obtained by the incoherent sparse design for $K = 4, 6, 8, 10$, and 12. One can see the influence of a proper choice of K on the performance, especially on the ability to obtain nearly constant and superior DF. One can see that $K = 10$ and $K = 12$ obtain similar performances. Thus, a practical procedure to set K is to design the beamformer for several values of K, and choose the one that yields the optimal performance. Note that for $K = 4$ and $K = 6$, superior WNG for high frequencies was obtained due to larger tolerance values of ϵ_1 and ϵ_2, but at the expense of much lower DF.

Fig. 9 shows the WNG and the DF as a function of frequency obtained by the incoherent sparse design for $\alpha = 0.45, 0.6, 0.7, 0.8$, and 0.9. One can see that the choice of $\alpha = 0.6$ yields a good compromise between the WNG and the DF.

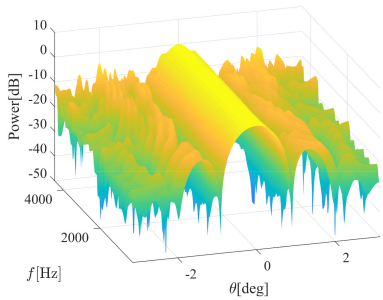

(a) incoherent sparse design

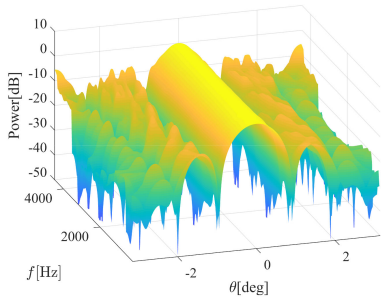

(b) coherent sparse design

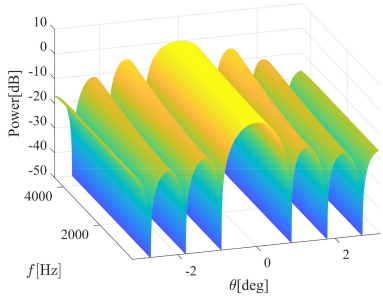

(c) MN design

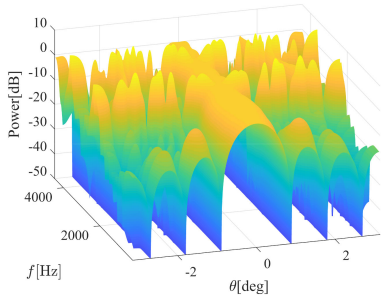

(d) MNE design

Fig. 7. Beampatterns versus frequency for the four examined design approaches.

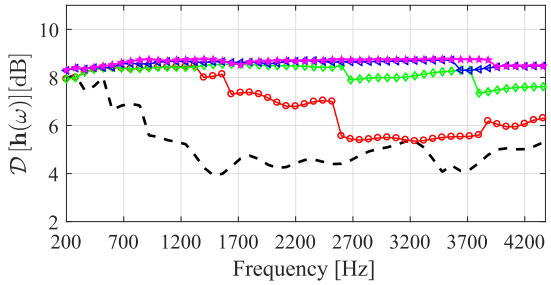

(a)

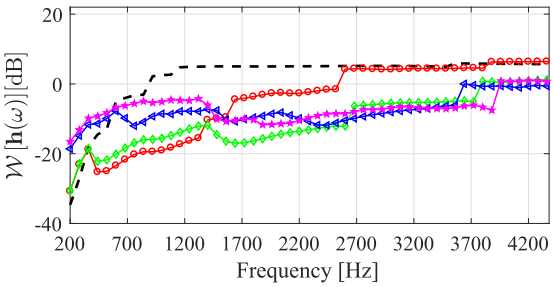

(b)

Fig. 8. (a) DF and (b) WNG vs. frequency obtained by the incoherent sparse design for the case that $K = 4$ (black dashed line), $K = 6$ (red circles line), $K = 8$ (green diamonds line), $K = 10$ (blue triangles line), and $K = 12$ (magenta stars line).

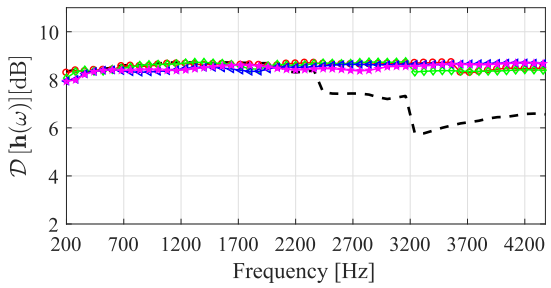

(a)

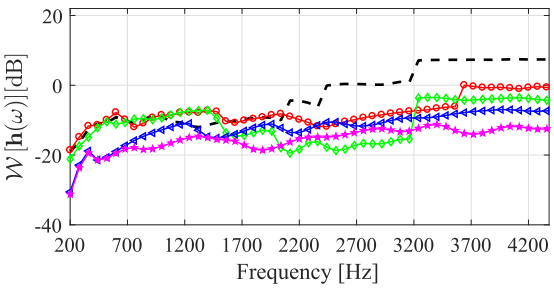

(b)

Fig. 9. (a) DF and (b) WNG vs. frequency obtained by the incoherent sparse design for the case that $\alpha = 0.45$ (black dashed line), $\alpha = 0.6$ (red circles line), $\alpha = 0.7$ (green diamonds line), $\alpha = 0.8$ (blue triangles line), and $\alpha = 0.9$ (magenta stars line).

B. Sparse Superdirective Planar Array

Let us now consider the problem of synthesizing a sparse planar array of sensors used for implementation of FI superdirective beamformer. Such a beamformer can be used for several applications like underwater acoustic sonar arrays. Herein, we focus only on the proposed incoherent design approach since for such a high number of potential sensors and frequency bins, the coherent processing is infeasible when using standard hardware while the proposed approach still yields results with a reasonable computational complexity.

We apply the design for the frequency range between $f_{\mathrm{low}} = 400$ Hz and $f_{\mathrm{high}} = 6000$ Hz. Assuming a typical duration of $T = 10$ msec for the window used for the analysis of

underwater acoustic signals, the frequency resolution is $\Delta f = 1/T = 100$ Hz. Thus, the number of bins J can be calculated as $J = \frac{f_{\rm high} - f_{\rm low}}{\Delta f} = 58$. For the incoherent sparse approach, an initial square array of 16×16 potential sensors (i.e., $M = 256$), with an element spacing of $\delta = 1.5$ cm $\ll \frac{2\pi c}{\omega_{\rm max}} \approx 5.5$ cm between two adjacent sensors is assumed.

We uniformly discretize the angular axis and the elevation axis with $\Delta\theta = 4^\circ$ and $\Delta\phi = 4^\circ$, respectively. Under the assumption that the plane of the array consolidates with the x-y plane, the wavenumber is

$$\mathbf{k}_{\omega_j}(\boldsymbol{\rho}) = -\frac{\omega_j}{c}\left[\cos\theta \sin\phi \sin\theta \sin\phi\right]^T. \tag{36}$$

The analytical expression of the superdirective beamformer is obtained by maximizing the DF (34) subject to the distortionless constraint in the desired signal direction, $\boldsymbol{\rho}_{\rm s}$, and for a given ω_j is [24]

$$\mathbf{h}_{\rm SD}(\omega_j) = \frac{\boldsymbol{\Gamma}^{-1}_{{\rm dn},\epsilon}(\omega_j)\mathbf{d}\left(\mathbf{k}_{\omega_j}(\boldsymbol{\rho}_{\rm s})\right)}{\mathbf{d}^H\left(\mathbf{k}_{\omega_j}(\boldsymbol{\rho}_{\rm s})\right)\boldsymbol{\Gamma}^{-1}_{{\rm dn},\epsilon}(\omega_j)\mathbf{d}\left(\mathbf{k}_{\omega_j}(\boldsymbol{\rho}_{\rm s})\right)}, \tag{37}$$

where $\boldsymbol{\Gamma}_{{\rm dn},\epsilon}(\omega_j)$ is a regularized version of $\boldsymbol{\Gamma}_{\rm dn}(\omega_j)$ (35), i.e.,

$$\boldsymbol{\Gamma}_{{\rm dn},\epsilon}(\omega_j) = \boldsymbol{\Gamma}_{\rm dn}(\omega_j) + \epsilon\mathbf{I}_M, \tag{38}$$

with the regularization parameter $\epsilon = 10^{-4}$.

We set the frequency $f_0 = 400$ Hz to be the reference frequency of the desired beampattern, i.e.,

$$\mathcal{B}_{\rm d}(\boldsymbol{\rho}) = \mathcal{B}(\mathbf{h}(\omega_0)) = \mathbf{h}^H(\omega_0)\mathbf{d}\left(\mathbf{k}_{\omega_0}(\boldsymbol{\rho})\right), \tag{39}$$

where $\omega_0 = 2\pi f_0$. Fig. 10 (a) presents in a logarithmic scale, the three-dimensional desired beampattern, $\mathcal{B}_{\rm d}(\boldsymbol{\rho})$, matched to the reference frequency of $f_0 = 400$ Hz . Note that even-though $\mathcal{B}_{\rm d}(\boldsymbol{\rho})$ has two mainlobes in opposite directions, practically it contains only one mainlobe steered towards the broadside while the opposite direction is blocked by the array plane and there is a negligible radiation in this direction.

We set empirically the number of sensors for the incoherent sparse design to be $K = 36$ sensors, and compare the incoherent approach with two uniform design approaches. In the first one, all the $K = 36$ sensors are placed in the center of the allowed aperture with an element spacing of $\delta = 1.5$ cm. Similarly to the linear case, very good FI and DF can be obtained at the expense of poor WNG. Therefore, the beamformer coefficients vector for that case was obtained by minimizing $\mathcal{C}_4$ (16) subject to $\mathcal{C}_1, \mathcal{C}_2, \mathcal{C}_3$ (12)–(15). We refer to this approach as the small aperture planar (SAP) array approach. The second uniform design approach may use the $K = 36$ sensors spread over the entire allowable aperture. The trends for this design are the opposite: high WNG but inferior DF, especially at high frequencies. Therefore, for this design we minimize $\mathcal{C}_1$ (12) subject to $\mathcal{C}_2, \mathcal{C}_3, \mathcal{C}_4$ (13)-(16). We refer to this approach as the large aperture planar (LAP) array.

Similarly to the previous example, we apply the parameters adjustment procedure proposed in Section VI to set the tolerance parameters. We get the initial values $\epsilon_1(\omega_1) = 0.6$, $\epsilon_2(\omega_1) = 2$, and $\gamma(\omega_1) \approx 3$, and the final values of $\epsilon_1(\omega_J) = 1.8$, $\epsilon_2(\omega_J) = 6$, and $\gamma(\omega_J) \approx 0.1$.

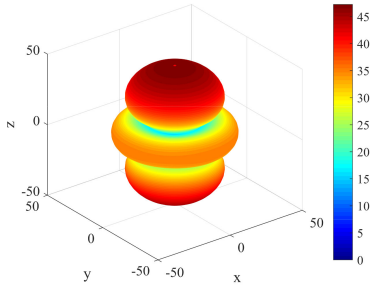

(a) Desired beampattern

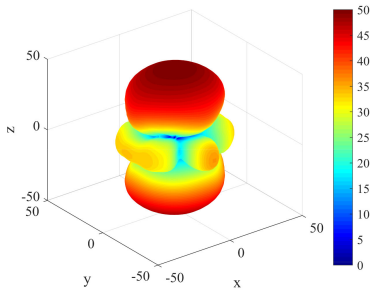

(b) Incoherent sparse design

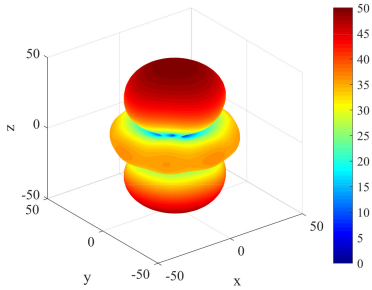

(c) SPA design

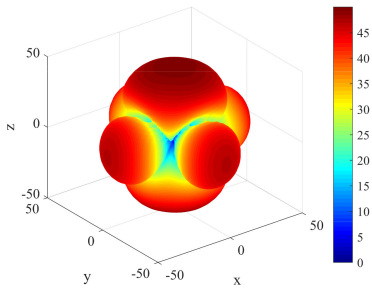

(d) LPA design

Fig. 10. Synthesized FI beampatterns for $f = 5100$ Hz using various approaches. Also presented is the desired beampattern, $\mathcal{B}_{\rm d}(\boldsymbol{\rho})$ matched to the reference frequency of $f_0 = 400$ Hz.

For simplicity, we may concentrate on beampatterns whose mainbeams are at the broadside, i.e., corresponding to $\phi_{\rm s} = 0^\circ$. Sparse designs of beampatterns steered to other directions are topics for future research. For this case, it is reasonable to assume that the beampatterns have symmetry with respect to the axes $x = 0$ and $y = 0$, i.e., all the four quarters combining the plane of the array are identical. Therefore, after the first analysis

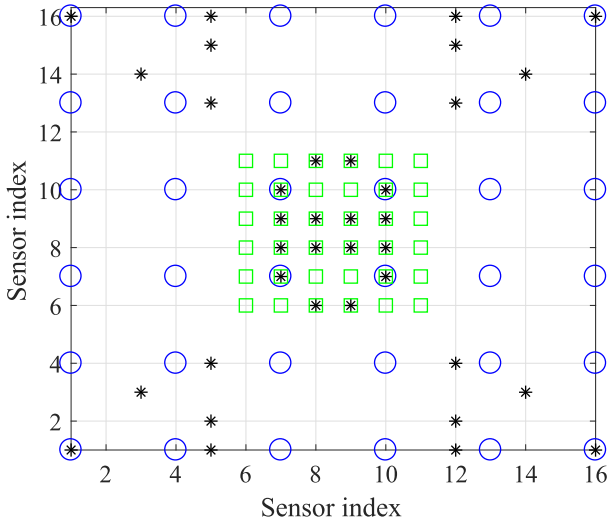

Fig. 11. The array layout of the planar array obtained by the incoherent proposed approach (black stars), the SAP uniform approach (green squares), and the LAP approach (blue circles).

step, we use the PCA algorithm to find only $K/4 = 9$ sensors in one of the quarters, and duplicate it to the three remaining quarters. Fig. 11 presents the array layout of the incoherent sparse approach (black stars), the SAP uniform design with small spacing (green squares), and the LAP design approach (blue circles).

In order to get more intuition regarding the sensors selected by the incoherent sparse design, we calculate the total energy of the coefficients of each sensor, that is

$$\mathcal{E}_m = \|\mathbf{H}_{\mathrm{A}}(m,:)\|_2^2, m = 1, 2, ..., M, \tag{40}$$

where $\mathbf{H}_{\mathrm{A}}(m,:)$ is the mth row of the matrix $\mathbf{H}_{\mathrm{A}}$. We define the log-ratio

$$\mathcal{L}_m = 10\log_{10}\frac{\mathcal{E}_m}{\max\limits_{m}\{\mathcal{E}_m\}_{m=1}^{M}}, \tag{41}$$

indicating how much dominant is the m th-sensor with respect to the other sensors by terms of the total energy it contains across the bandwidth of interest Ω, and define a threshold parameter T_0 such that sensors whose log-ratio satisfy $\mathcal{L}_m \leq T_0$ are ignored. In Fig. 12 one can see the selected sensors for the choice of (a) $T_0 = -5$ dB, (b) $T_0 = -7$ dB, (c) $T_0 = -10$ dB, and (d) $T_0 = -12$ dB. We can see from (a) that the most dominant sensors lay in the center and in the distant corners. As we decrease T_0, more sensors are added as illustrated in (b)–(d).

Fig. 13 shows the WNG (17) and the DF (34) as a function of the frequency obtained by the incoherent sparse design (black dashed line), the LAP design (blue triangles line), and the SAP design (green diamonds line). Also presented is the DF of the desired beampattern (magenta stars line). Like in the previous example, the incoherent sparse design is a good solution and optimal in terms of WNG and DF.

Figures 10(b)–(d) show synthesized FI beampatterns for $f = 5100$ Hz using the incoherent approach, the SPA approach, and the LPA approach.

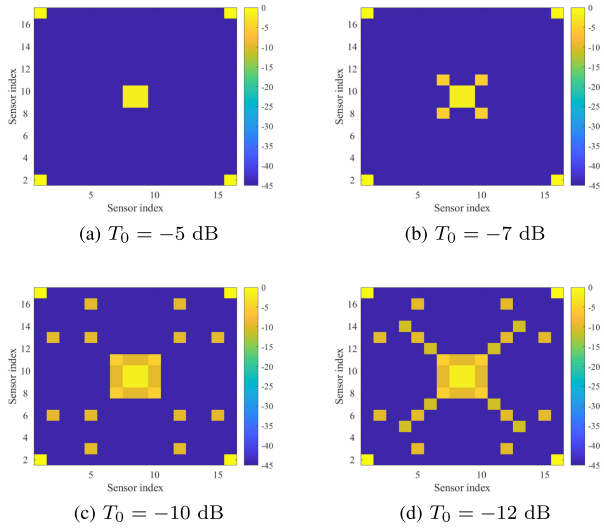

(a) $T_0 = -5$ dB (b) $T_0 = -7$ dB

(c) $T_0 = -10$ dB (d) $T_0 = -12$ dB

Fig. 12. Sensors chosen for different values of the threshold value T_0.

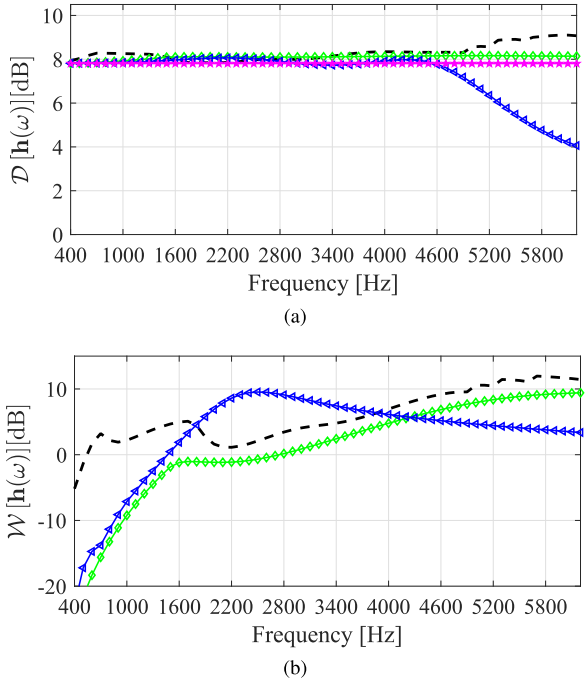

Fig. 13. (a) DF and (b) WNG vs. frequency obtained by the incoherent sparse design (black dashed line), the LAP design (blue triangles line), and the SAP design (green diamonds line). Also presented is the DF of the desired beampattern (magenta stars line).

The above design examples demonstrate the feasibility and the advantages of the incoherent approach compared to the coherent sparse design approach and to the uniform design approaches.

Note that for both the coherent and incoherent designs, it was assumed that the direction of the source, ρ_{s}, is given and the design depends on it, meaning that once the source direction is changed, the design is not valid anymore. A more sophisticated sparse design for geometries such as circular and concentric arrays, that can be steered in multiple directions, is currently under research.

VIII. Conclusion

We have presented an incoherent approach for a sparse design of FI beamformers, where the sensors positions are sparsely selected for each frequency bin separately, and subsequently a fusion mechanism is applied in order to determine the sensors used jointly for all frequencies in order to synthesize the FI beamformer. The proposed approach was applied to design robust superdirective FI beamformers with minimal number of sensors. It was compared to the coherent approach where optimization is performed simultaneously over all directions and frequencies of interest, and also to uniform design approaches. Simulations show that the proposed incoherent sparse design is a good compromise between robustness and directivity and obtains FI beamformer with significantly reduced computational complexity. Moreover, for scenarios where a large number of potential sensors and frequency bins is assumed, the coherent approach is infeasible while the incoherent design provides results with a reasonable computation time. Future research may focus on different array geometries, applying nonlinear dimension reduction techniques, as well as greedy-based algorithms for sparse design.

References

[1] M. Branstein and D. B. Ward, Eds, *Microphone Arrays: Signal Processing Techniques and Applications*. Berlin, Germany: Springer-Verlag, 2001.

[2] J. Benesty, J. Chen, Y. Huang, and J. Dmochowski, "On microphone-array beamforming from a MIMO acoustic signal processing perspective," *IEEE Trans. Audio, Speech, Lang. Process.*, vol. 15, no. 3, pp. 1053–1065, Mar. 2007.

[3] J. Benesty, J. Chen, and Y. Huang, *Microphone Array Signal Processing*. Berlin, Germany: Springer-Verlag, 2008.

[4] S. Yan, "Optimal design of FIR beamformer with frequency invariant patterns," *Appl. Acoust.*, vol. 67, pp. 511–528, 2006.

[5] E. Mabande, A. Schad, and W. Kellermann, "Design of robust superdirective beamformer as a convex optimization problem," in *Proc. IEEE Int. Conf. Acoust. Specch Signal Process.*, Taipei, Taiwan, 2009, pp. 77–80.

[6] H. H. Chen, S. C. Chan, and K. L. Ho, "Adaptive beamforming using frequency invariant uniform concentric circular arrays," *IEEE Trans. Circuits Syst. I, Reg. Papers*, vol. 54, no. 9, pp. 1938–1949, Sep. 2007.

[7] S. C. Chan and H. H. Chen, "Uniform concentric circular arrays with frequency-invariant characteristics—Theory, design, adaptive beamforming and doa estimation," *IEEE Trans. Signal Process.*, vol. 55, no. 1, pp. 165–177, Jan. 2007.

[8] W. Liu and S. Weiss, *Wideband Beamforming: Concepts and Techniques*. Chichester, U.K.: Wiley, 2010.

[9] M. Crocco and A. Trucco, "Design of robust superdirective arrays with a tunable tradeoff between directivity and frequency-invariance," *IEEE Trans. Signal Process.*, vol. 59, no. 5, pp. 2169–2181, May 2011.

[10] B. D. Van Veen and K. V. Buckley, "Beamforming: A versatile approach to spatial filtering," *IEEE Mag. Acoust., Speech, Signal Process.*, vol. 5, no. 2, pp. 4–24, Apr. 1988.

[11] W. Liu and S. Weiss, "Design of frequency invariant beamformers for broadband arrays," *IEEE Trans. Signal Process.*, vol. 56, no. 2, pp. 855–860, Feb. 2008.

[12] T. Do-Hong and P. Russer, "Spatial signal processing for wideband beamforming," in *Proc. 7th Int. Symp. Theor. Elect. Eng.*, 2003, pp. 73–76.

[13] H. Hung and M. Kaveh, "Focusing matrices for coherent signal subspace processing," *IEEE Trans. Acoust. Speech Signal Process.*, vol. 36, no. 8, pp. 1272–1281, Aug. 1988.

[14] M. A. Doron and A. Nevet, "Robust wavefield interpolation for adaptive wideband beamforming," *Signal Process.*, vol. 80, pp. 1579–1594, 2008.

[15] Y. Buchris, I. Cohen, and M. A. Doron, "Bayesian focusing for coherent wideband beamforming," *IEEE Trans. Audio, Speech, Lang. Process.*, vol. 20, no. 4, pp. 1282–1295, May 2012.

[16] J. Benesty and J. Chen, *Study and Design of Differential Microphone Arrays*. Berlin, Germany: Springer-Verlag, 2012.

[17] J. Benesty, J. Chen, and I. Cohen, *Design of Circular Differential Microphone Arrays*. Berlin, Germany: Springer-Verlag, 2015.

[18] G. W. Elko, "Superdirectional microphone arrays," in *Acoustic Signal Processing for Telecommunication*, S. L. Gay and J. Benesty, Eds. Boston, MA, USA: Kluwer, 2000, ch. 10, pp. 181–237.

[19] H. Teutsch and G. W. Elko, "First- and second-order adaptive differential microphone arrays," in *Proc. 7th Int. Workshop Acoust. Echo Noise Control*, 2001, pp. 57–60.

[20] M. Buck, "Aspects of first-order differential microphone arrays in the presence of sensor imperfections," *Eur. Trans. Telecommun.*, vol. 13, pp. 115–122, Mar. 2002.

[21] E. De Sena, H. Hacihabiboğlu, and Z. Cavetković, "On the design and implementation of higher order differential microphones," *IEEE Trans. Audio, Speech, Lang. Process.*, vol. 20, no. 1, pp. 162–174, Jan. 2012.

[22] L. Zhao, J. Benesty, and J. Chen, "Design of robust differential microphone arrays," *IEEE/ACM Trans. Audio, Speech, Lang. Process.*, vol. 22, no. 10, pp. 1455–1464, Oct. 2014.

[23] C. Pan, J. Benesty, and J. Chen, "Design of robust differential microphone arrays with orthogonal polynomials," *J. Acoust. Soc. Amer.*, vol. 138, no. 2, pp. 1079–1089, Aug. 2015.

[24] H. Cox, R. M. Zeskind, and T. Kooij, "Practical supergain," *IEEE Trans. Acoust., Speech, Signal Process.*, vol. ASSP-34, no. 3, pp. 393–398, June 1986.

[25] M. I. Skolnik, G. Nemhauser, and J. W. Sherman, III, "Dynamic programming applied to unequally spaced arrays," *IEEE Trans. Antennas Propag.*, vol. AP-12, no. 1, pp. 35–43, Jan. 1964.

[26] O. M. Bucci, M. D'Urso, T. Isernia, P. Angeletti, and G. Toso, "Deterministic synthesis of uniform amplitude sparse arrays via new density taper techniques," *IEEE Trans. Antennas Propag.*, vol. 58, no. 6, pp. 1949–1958, Jun. 2010.

[27] O. Quevedo-Teruel and E. Rajo-Iglesias, "Ant colony optimization in thinned array synthesis with minimum sidelobe level," *IEEE Trans. Antennas Wireless Propag. Lett.*, vol. 5, pp. 349–352, 2006.

[28] A. Trucco, E. Omodei, and P. Repetto, "Synthesis of sparse planar arrays," *Electron. Lett.*, vol. 33, no. 22, pp. 1834–1835, Oct. 1997.

[29] R. M. Leahy and B. D. Jeffs, "On the design of maximally sparse beamforming arrays," *IEEE Trans. Antennas Propag.*, vol. 39, no. 8, pp. 1178–1187, Aug. 1991.

[30] Y. Liu, Q. H. Liu, and Z. Nie, "Reducing the number of elements in the synthesis of shaped-beam patterns by the forward-backward matrix pencil method," *IEEE Trans. Antennas Propag.*, vol. 58, no. 2, pp. 604–608, Feb. 2010.

[31] W. Zhang, L. Li, and F. Li, "Reducing the number of elements in linear and planar antenna arrays with sparseness constrained optimization," *IEEE Trans. Antennas Propag.*, vol. 59, no. 8, pp. 3106–3111, Feb. 2011.

[32] G. Oliveri, E. T. Bekele, F. Robol, and A. Massa, "Sparsening conformal arrays through a versatile BCS-based method," *IEEE Trans. Antennas Propag.*, vol. 62, no. 4, pp. 1681–1689, Apr. 2014.

[33] B. Fuchs, "Synthesis of sparse arrays with focused or shaped beampattern via sequential convex optimizations," *IEEE Trans. Antennas Propag.*, vol. 60, no. 7, pp. 3499–3503, Jul. 2012.

[34] M. D'Urso, G. Prisco, and R. M. Tumolo, "Maximally sparse, steerable, and nonsuperdirective array antennas via convex optimizations," *IEEE/ACM Trans. Antennas Propag.*, vol. 64, no. 9, pp. 800–815, Sep. 2016.

[35] S. E. Nai, W. Ser, Z. L. Yu, and H. Chen, "Beampattern synthesis for linear and planar arrays with antenna selsction by convex optimization," *IEEE Trans. Antennas Propag.*, vol. 58, no. 12, pp. 3923–3930, Dec. 2010.

[36] M. Crocco and A. Trucco, "Design of superdirective planar arrays with sparse aperiodic layouts for processing broadband signals via 3-d beamforming," *IEEE/ACM Trans. Audio, Speech, Lang. Process.*, vol. 22, no. 4, pp. 800–815, Apr. 2014.

[37] T. Chou, "Frequency-independent beamformer with low response error," in *Proc. IEEE Int. Conf. Acoust. Specch Signal Process.*, Detroit, MI, USA, May 1995, pp. 2995–2998.

[38] Y. R. Zheng, R. A. Goubran, and M. El-Tanany, "Experimental evaluation of a nested microphone array with adaptive noise cancellers," *IEEE Trans. Instrum. Meas.*, vol. 53, no. 3, pp. 777–786, Jun. 2004.

[39] I. J. H. Doles and F. D. Benedict, "Broad-band array design using the asymptotic theory of unequally spaced arrays," *IEEE Trans. Antennas Propag.*, vol. AP-36, no. 1, pp. 27–33, Jan. 1988.

[40] D. B. Ward, R. A. Kennedy, and R. C. Williamson, "Theory and design of broadband sensor arrays with frequency invariant farfield beam-patterns," *J. Acoust. Soc. Amer.*, vol. 97, no. 2, pp. 1023–1034, Feb. 1995.

[41] M. Crocco and A. Trucco, "Stochastic and analytic optimization of sparse aperiodic arrays and broadband beamformers with robust superdirective patterns," *IEEE Trans. Audio, Speech, Lang. Process.*, vol. 20, no. 9, pp. 2433–2447, Nov. 2012.
[42] Z. Li, K. F. Cedric Yiu, and Z. Fen, "A hybrid descent method with genetic algorithm for microphone array placement design," *Appl. Soft Comput.*, vol. 13, pp. 1486–1490, 2013.
[43] Y. Liu, L. Zhang, C. Zhu, and Q. H. Liu, "Synthesis of nonuniformly spaced linear arrays with frequency-invariant patterns by the generalized matrix pencil methods," *IEEE Trans. Antennas Propag.*, vol. 63, no. 4, pp. 1614–1625, Apr. 2015.
[44] M. B. Hawes and W. Liu, "Sparse array design for wideband beamforming with reduced complexity in tapped delay-lines," *IEEE/ACM Trans. Audio, Speech, Lang. Process.*, vol. 22, no. 8, pp. 1236–1247, Aug. 2014.
[45] Y. Liu, L. Zhang, L. Ye, Z. Nie, and Q. H. Liu, "Synthesis of sparse arrays with frequency-invariant-focused beam patterns under accurate sidelobe control by iterative second-order cone programming," *IEEE Trans. Antennas Propag.*, vol. 63, no. 12, pp. 5826–5832, Dec. 2015.
[46] S. F. Cotter, B. D. Rao, K. Engan, and K. Kreutz-Delgado, "Sparse solutions to linear inverse problems with multiple measurement vectors," *IEEE Trans. Signal Process.*, vol. 53, no. 7, pp. 2477–2488, Jul. 2005.
[47] H. L. Van-trees, *Detection, Estimation and Modulation Theory, Part IV - Optimum Array Processing*. New York, NY, USA: Wiley, 2002.
[48] E. J. Candès, M. B. Wakin, and S. P. Bond, "Enhancing sparsity by reweighted ℓ_1 minimization," *J. Fourier Anal. Appl.*, vol. 14, pp. 877–905, Dec. 2008.
[49] P. T. Boufounosa, P. Smaragdisb, and B. Rajc, "Joint sparsity models for wideband array processing," *Proc. SPIE*, vol. 8138, pp. 81 380K, 2011.
[50] M. Grant, S. Boyd, and Y. Ye, "CVX: MATLAB software for disciplined convex programming," 2008.
[51] I. Jolliffe, *Principal Component Analysis. Springer Series in Statistics*. New York, NY, USA: Springer, 1986.
[52] J. A. Hartigan and M. A. Wong, "Algorithm as 136: A k-means clustering algorithm," *J. Roy. Statist. Soc. C (Appl. Statist.)*, vol. 28, no. 1, pp. 100–108, 1979.
[53] C. Ding and X. He, "K-means clustering via principal component analysis," in *Proc. 21st Int. Conf. Mach. Learn.*, 2004, pp. 29–36.

Yaakov Buchris received the B.Sc. and M.Sc. degrees in electrical engineering in 2005 and 2011, respectively, from the Technion-Israel Institute of Technology, Haifa, Israel, where he is currently working toward the Ph.D. degree in electrical engineering.

Since 2002, he has been with RAFAEL, Advanced Defense Systems, Ltd, Haifa, Israel, as a Research Engineer in the Underwater Acoustic Communication Group. Since 2005, he has also been a Teaching Assistant and a Project Supervisor with the Communications Lab and the Signal and Image Processing Lab, Electrical Engineering Department, Technion-Israel Institute of Technology. His research interests include statistical signal processing, adaptive filtering, digital communications, and array processing.

Alon Amar (S'04–M'09) received the B.Sc. degree in electrical engineering from the Technion-Israel Institute of Technology, Haifa, Israel, in 1997 and the M.Sc. degree in electrical engineering from Tel Aviv University, Tel Aviv, Israel, in 2003, and 2009, respectively. From 2009 to 2010, he was a Postdoctoral Research Associate with the Circuits and Systems Group, Faculty of Electrical Engineering, Mathematics, and Computer Science, Delft University of Technology, Delft, The Netherlands. In 2011, he joined the Israeli National Research Center, Haifa, as a Research Scientist. Since 2016, he has been an Adjunct Lecturer and a Research Associate with the Department of Electrical Engineering, Technion, Israel Institute of Technology. His main research interests include statistical and array signal processing, wireless communication, and sensor networks.

Jacob Benesty received the master's degree in microwaves from Pierre and Marie Curie University, Paris, France, in 1987, and the Ph.D. degree in control and signal processing from Orsay University, Orsay, France, in April 1991.

During his Ph.D. (from November 1989 to April 1991), he worked on adaptive filters and fast algorithms with the Centre National d'Etudes des Telecomunications, Paris, France. From January 1994 to July 1995, he was with the Telecom Paris University on multichannel adaptive filters and acoustic echo cancellation. From October 1995 to May 2003, he was first a Consultant and then a Member of the Technical Staff with the Bell Laboratories, Murray Hill, NJ, USA. In May 2003, he joined the INRS-EMT, University of Quebec, Montreal, QC, Canada, as a Professor. He is currently a Visiting Professor with the Technion-Israel Institute of Technology, Haifa, Israel, and an Adjunct Professor with the Aalborg University, Aalborg, Denmark. His research interests include signal processing, acoustic signal processing, and multimedia communications. He is the inventor of many important technologies. In particular, he was the Lead Researcher with the Bell Labs who conceived and designed the world-first real-time hands-free full-duplex stereophonic teleconferencing system. Also, he conceived and designed the world-first PC-based multiparty hands-free full-duplex stereo conferencing system over IP networks.

Dr. Benesty is currently the Editor for the book series Springer Topics in Signal Processing. He was the General Chair and the Technical Chair of many international conferences and a member of several IEEE technical committees. Four of his journal papers were awarded by the IEEE Signal processing Society and in 2010 he received the Gheorghe Cartianu Award from the Romanian Academy. He has coauthored and coedited/coauthored numerous books in the area of acoustic signal processing.

Israel Cohen (M'01–SM'03–F'15) He received the B.Sc. (*Summa Cum Laude*), M.Sc., and Ph.D. degrees in electrical engineering from the Technion – Israel Institute of Technology, Haifa, Israel, in 1990, 1993, and 1998, respectively.

He is currently a Professor of electrical engineering with the Technion – Israel Institute of Technology. From 1990 to 1998, he was a Research Scientist with RAFAEL Research Laboratories, Israel Ministry of Defense, Haifa. From 1998 to 2001, he was a Postdoctoral Research Associate with the Computer Science Department, Yale University, New Haven, CT, USA. In 2001, he joined the Electrical Engineering Department, Technion – Israel Institute of Technology. He is a coeditor of the Multichannel Speech Processing Section of the *Springer Handbook of Speech Processing* (Springer, 2008), and a coauthor of *Fundamentals of Signal Enhancement and Array Signal Processing* (Wiley-IEEE Press, 2017). His research interests include array processing, statistical signal processing, analysis and modeling of acoustic signals, speech enhancement, noise estimation, microphone arrays, source localization, blind source separation, system identification, and adaptive filtering.

Dr. Cohen was awarded the Norman Seiden Prize for Academic Excellence (2017), the SPS Signal Processing Letters Best Paper Award (2014), the Alexander Goldberg Prize for Excellence in Research (2010), and the Muriel and David Jacknow Award for Excellence in Teaching (2009). He is currently an Associate Member of the IEEE Audio and Acoustic Signal Processing Technical Committee. He was an Associate Editor for the IEEE TRANSACTIONS ON AUDIO, SPEECH, AND LANGUAGE PROCESSING and the IEEE SIGNAL PROCESSING LETTERS, and as Member of the IEEE Audio and Acoustic Signal Processing Technical Committee and the IEEE Speech and Language Processing Technical Committee.